# Supplementary Information

## Hierarchical chirality transfer in the growth of *Towel Gourd* tendrils

Jian-Shan Wang[1,2*], Gang Wang[3], Xi-Qiao Feng[4†], Takayuki Kitamura[2], Yi-Lan Kang[1], Shou-Wen Yu[4], Qing-Hua Qin[5]

[1] Tianjin Key Laboratory of Modern Engineering Mechanics, Department of Mechanics, Tianjin University, Tianjin 300072, People's Republic of China

[2] Department of Mechanical Engineering and Science, Kyoto University, Nishikyo-ku, Kyoto 615-8540, Japan

[3] School of Materials Science and Engineering, Shanghai University, Shanghai 200444, People's Republic of China

[4] AML and CNMM, Department of Engineering Mechanics, Tsinghua University, Beijing 100084, People's Republic of China

[5] Research School of Engineering, Australian National University, Canberra, ACT 0200, Australia

[*] e-mail: wangjs@tju.edu.cn

[†] e-mail: Fengxq@tsinghua.edu.cn

## Theoretical model

### S1 Intrinsic torsion of tendril filaments

As shown in Fig. 5, the shape change of a cellulose fibril during deswelling can produce an internal torque $M$ that acts on the cell. Following the Cosserat rod model of a spring [1, 2], the torque $M$ can be expressed as

$$M = B'\hat{\psi}_0(\cos\alpha - \cos\alpha_0)\cos\alpha + C'\hat{\psi}_0(\sin\alpha - \sin\alpha_0)\sin\alpha\,, \tag{S1}$$

where $B' = \frac{1}{4}E\pi r_0^4$ is the bending stiffness of the tendril cell, $C' = \frac{1}{2}G\pi r_0^4$ the torsion rigidity, and $\hat{\psi}_0 = \partial\psi/\partial s = \sin\alpha_0/R_0'$, where $\psi$ is the Euler angle, $s$ is the arc length of cellulose fibril, $R_0'$ is the initial helical radius of the cellulose fibril helix, $r_0$ is the radius of the cross section of the cellulose fibril, and $\alpha_0$ and $\alpha$ are the helical angle of the fully swelled and partially deswelled cellulose fibril helices, respectively. Considering the cell bundle structures of the tendril filament (Fig. 4), the distributed torque $m_0$ acting on the tendril filament per unit length is determined as follows:

$$m_0 = \frac{Mr_2^2}{2\pi R_0' r_1^2 \tan\alpha}\,, \tag{S2}$$

where $r_1$ and $r_2$ are the radii of the cell and the tendril filament, respectively, $R_0'$ is the helical radius of the cellulose fibril helix. During growth or swelling/deswelling of a tendril, the torque $m_0$ will produce an intrinsic torsion deformation of the tendrilfilament. Thus, the reorientation of cellulose fibrils provide a driving force for the formation and evolution of the tendril helix.

### S2 Constitutive relationship

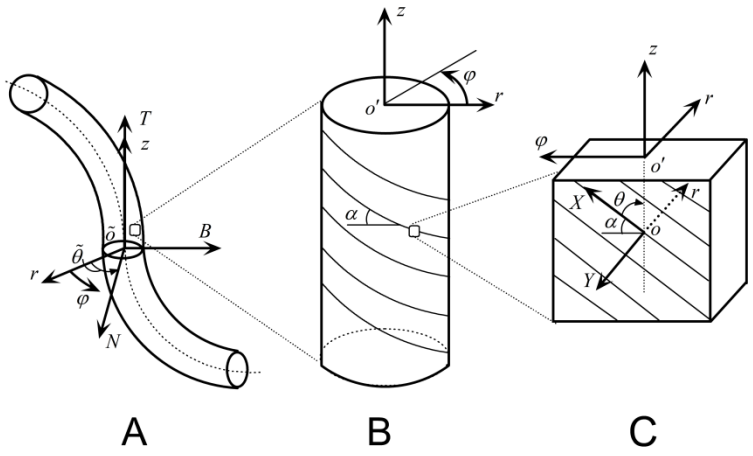


Fig. S1. Coordinate systems: (*A*) Frenet coordinate system (FCS) with base vectors $\boldsymbol{e}_N$, $\boldsymbol{e}_B$ and $\boldsymbol{e}_T$. (*B*) Cylinder coordinate system (CCS) with basis vectors $\boldsymbol{e}_r$, $\boldsymbol{e}_\varphi$ and $\boldsymbol{e}_z$; (*C*) Helical coordinate system (HCS) with basis vectors $\boldsymbol{e}_L$, $\boldsymbol{e}_T$ and $\boldsymbol{e}_r$.

In the wall of a tendril cell, cellulose fibril helices are closed packed, as shown in Fig. 3. Thus, the cell wall can be considered to be an orthotropic layer. Referring to the helical coordinate system (HCS) ($o-XYr$)shown in Fig. S1*C*, in which the $X$ axis is oriented in the winding direction of the cellulose fibril, the $r$ axis is oriented in the direction of the cell wall thickness, and $Y$ is perpendicular to the $X$ and $r$ axes. The orthotropic layer forms a cylindrical tube that is oriented parallel to a certain direction, for which we establish the cylindrical coordinate system (CCS) ($o'-r\varphi z$). The $r$ axis is oriented in the radial direction of the cell cylinder and the same as that in HCS, and the $z$ and $\varphi$ axes are oriented in the axial and angular directions of the cylinder, respectively. Furthermore, the tendril filament is curved into a spatial morphology and is treated here as a Kirchhoff rod having a helical microstructure. For such a spatially curved rod, we introduce a Frenet coordinate system (FCS) ($o-TBN$) shown in Fig. S1*A*, in which the origin $o$ is located at the centerline of the tendril filament, both the $z$ and $T$ axes are oriented in the tangent

direction of the centerline, and the $N$ and $B$ axes are oriented in the normal and binormal directions of the centerline, respectively.

The constitutive relation of the helical orthotropic layer in HCS is [3]

$$\{\boldsymbol{\sigma}\}_{\mathrm{HCS}} = [\boldsymbol{Q}]\{\boldsymbol{\varepsilon}\}_{\mathrm{HCS}}, \tag{S3}$$

where $\{\boldsymbol{\sigma}\}_{\mathrm{HCS}}$ is the stress matrix and $\{\boldsymbol{\varepsilon}\}_{\mathrm{HCS}}$ is the strain matrix. The subscript HCS indicates the parameters defined in the helical coordinate system. $[\boldsymbol{Q}]$ is the orthotropic elastic stiffness matrix, which is expressed as

$$[\boldsymbol{Q}] = \begin{bmatrix} Q_{11} & Q_{12} & Q_{13} & 0 & 0 & 0 \\ Q_{12} & Q_{22} & Q_{23} & 0 & 0 & 0 \\ Q_{13} & Q_{23} & Q_{33} & 0 & 0 & 0 \\ 0 & 0 & 0 & Q_{44} & 0 & 0 \\ 0 & 0 & 0 & 0 & Q_{55} & 0 \\ 0 & 0 & 0 & 0 & 0 & Q_{66} \end{bmatrix}. \tag{S4}$$

Through coordinate transformation, we can obtain the constitutive relationship in the cylindrical coordinate system (CCS) from equation S3 as

$$\{\boldsymbol{\sigma}\}_{\mathrm{CCS}} = \left[\bar{\boldsymbol{Q}}\right]\{\boldsymbol{\varepsilon}\}_{\mathrm{CCS}}, \tag{S5}$$

where the subscript CCS stands for the parameters in the cylinder coordinate system. The stiffness matrix, $\left[\bar{\boldsymbol{Q}}\right]$, is written as

$$\left[\bar{\boldsymbol{Q}}\right] = \left[\boldsymbol{T}^{-1}\right][\boldsymbol{Q}]\left[\boldsymbol{T}^{-1}\right]^{\mathrm{T}}, \tag{S6}$$

where the subscript T denotes the transformation matrix, and

$$\left[\boldsymbol{T}^{-1}\right]=\begin{bmatrix} m^2 & n^2 & 0 & 0 & 0 & -2mn \\ n^2 & m^2 & 0 & 0 & 0 & 2mn \\ 0 & 0 & 1 & 0 & 0 & 0 \\ 0 & 0 & 0 & m & n & 0 \\ 0 & 0 & 0 & -n & m & 0 \\ mn & -mn & 0 & 0 & 0 & m^2-n^2 \end{bmatrix}, \tag{S7}$$

Here, $m=\cos\theta$, $n=\sin\theta$, and $\theta$ is the angle measured from the *L* axis to the *z* axis, and $\alpha$ the helical angle of a cellulose fibril. Moreover, $\theta$ and $\alpha$ satisfy the relationship $\theta+\alpha=90^{\circ}$.

The matrix $\left[\bar{\boldsymbol{Q}}\right]$ can obtained from equations **S6** and **S7** as follows:

$$\left[\bar{\boldsymbol{Q}}\right]=\begin{bmatrix} \bar{Q}_{11} & \bar{Q}_{12} & \bar{Q}_{13} & 0 & 0 & \bar{Q}_{16} \\ \bar{Q}_{12} & \bar{Q}_{22} & \bar{Q}_{23} & 0 & 0 & \bar{Q}_{26} \\ \bar{Q}_{13} & \bar{Q}_{23} & \bar{Q}_{33} & 0 & 0 & \bar{Q}_{36} \\ 0 & 0 & 0 & \bar{Q}_{44} & 0 & 0 \\ 0 & 0 & 0 & 0 & \bar{Q}_{55} & 0 \\ \bar{Q}_{16} & \bar{Q}_{26} & \bar{Q}_{36} & 0 & 0 & \bar{Q}_{66} \end{bmatrix}. \tag{S8}$$

A tendril filament can be regarded as an elastic rod with spatial configuration. Using coordinate transformation, we obtain the constitutive relation of tendril filaments in the Frenet coordinate system:

$$\left\{\boldsymbol{\sigma}\right\}_{\mathrm{FNT}}=\left[\boldsymbol{Q}\right]\left\{\boldsymbol{\varepsilon}\right\}_{\mathrm{FNT}}, \tag{S9}$$

where the subscript FNT indicates the Frenet coordinate system. The elastic stiffness matrix $\left[\boldsymbol{Q}\right]$ is related to $\left[\bar{\boldsymbol{Q}}\right]$ via the relation

$$\left[\boldsymbol{Q}\right]=\left[\boldsymbol{M}\right]\left[\bar{\boldsymbol{Q}}\right]\left[\boldsymbol{M}^{-1}\right] \tag{S10}$$

Here, $\left[\boldsymbol{M}\right]$ is the coordinate transfer matrix:

$$[\boldsymbol{M}]=\begin{bmatrix} 1 & 0 & 0 & 0 & 0 & 0 \\ 0 & \tilde{m}^2 & \tilde{n}^2 & 2\tilde{m}\tilde{n} & 0 & 0 \\ 0 & \tilde{n}^2 & \tilde{m}^2 & -2\tilde{m}\tilde{n} & 0 & 0 \\ 0 & -\tilde{m}\tilde{n} & \tilde{m}\tilde{n} & \tilde{m}^2-\tilde{n}^2 & 0 & 0 \\ 0 & 0 & 0 & 0 & \tilde{m} & -\tilde{n} \\ 0 & 0 & 0 & 0 & \tilde{n} & \tilde{m} \end{bmatrix} \tag{S11}$$

where $m=\cos\theta$, $n=\sin\theta$, and $\theta$ is the angle measured from the *N* axis to the *r* axis.

Since the tendril filament is very thin and slender, the strain moments on its cross-section can be approximated as constants. By averaging over the cylindrical volume ($V_0=2\pi R_0'\tan\alpha\cdot\pi R_0'^2$) containing one coil of cellulose fibril helix, the constitutive relation in equation (9) becomes

$$\{\boldsymbol{\sigma}'\}=[\boldsymbol{Q}']\{\boldsymbol{\varepsilon}\}_{\mathrm{FNT}}, \tag{S12}$$

where

$$\sigma_i'=\frac{1}{V_0}\int_0^{2\pi}\int_0^{R_0'}\int_0^{2\pi R_0'\tan\alpha}\sigma_i^{\mathrm{FNT}}r\mathrm{d}r\mathrm{d}\theta\mathrm{d}z, \tag{S13}$$

$$Q_{ij}'=\frac{1}{V_0}\int_0^{2\pi}\int_0^{R_0'}\int_0^{2\pi R_0'\tan\alpha}\tilde{Q}_{ij}r\mathrm{d}r\mathrm{d}\theta\mathrm{d}z=\frac{1}{2\pi}\int_0^{2\pi}Q_{ij}'\mathrm{d}\theta. \tag{S14}$$

Based on equation S14, we obtains

$$\begin{aligned} &Q_{11}'=\bar{Q}_{11},\quad Q_{12}'=Q_{21}'=Q_{13}'=Q_{31}'=\tfrac{1}{2}(\bar{Q}_{12}+\bar{Q}_{13}),\\ &Q_{22}'=Q_{33}'=\tfrac{1}{8}(3\bar{Q}_{22}+2\bar{Q}_{23}+3\bar{Q}_{33}),\ Q_{23}'=Q_{32}'=\tfrac{1}{8}(\bar{Q}_{22}+6\bar{Q}_{23}+\bar{Q}_{33}),\\ &Q_{44}'=\tfrac{1}{8}(3\bar{Q}_{22}+\bar{Q}_{33}-2\bar{Q}_{23}+\bar{Q}_{44}),\ Q_{55}'=Q_{66}'=\tfrac{1}{2}(\bar{Q}_{55}+\bar{Q}_{66}). \end{aligned} \tag{S15}$$

Equation S12 provides the constitutive relation of a tendril filament with the effect of cellulose fibril helices.

**S3 Elastic rod model of the tendril filament**

In the present study, a tendril filament with a circular cross section is treated as a Kirchhoff rod with helical microstructure. According to the Kirchhoff rod model, the strain components in the helical tendril can be expressed as [4, 5]

$$\begin{aligned}&\varepsilon_1=\varepsilon_2=0,\ \ \varepsilon_3=\omega_1 y-\omega_2 x,\ \ \gamma_{12}=\gamma_{21}=0,\\&\gamma_{13}=-\omega_1 z+\omega_3 y,\ \gamma_{23}=\gamma_{32}=\omega_3 x+\omega_1 y.\end{aligned} \tag{S16}$$

Based on equations S12 and S15, the stress components are obtained as

$$\begin{aligned}&\sigma_1=\sigma_2=0,\ \ \sigma_3=Q'_{11}(\omega_1 y-\omega_2 x),\ \ \tau_{12}=\tau_{21}=0,\\&\tau_{13}=\tau_{31}=Q'_{55}\omega_3 y,\ \ \tau_{23}=\tau_{32}=Q'_{55}(\omega_3 x+\omega_1 y).\end{aligned} \tag{S17}$$

Then, the potential energy function $\Pi$ of a tendril filament of length $L_0$ is

$$\Pi=\int_0^{L_0}\left[H_0(\kappa(s),\tau(s))-W_0(s)\right]\mathrm{d}s, \tag{S18}$$

where $\kappa(s)$ and $\tau(s)$ are the curvature and torsion of the tendril filament, respectively. $H_0$ is the strain energy of the tendril filament, and $W_0$ the potential energy of external force, which can be written as

$$\begin{aligned}&H_0=\frac{1}{2}\left\{B(\alpha)\left[\kappa(s)-\kappa_0(s)\right]^2+C(\alpha)\left[\tau(s)-\tau_0(s)\right]^2\right\},\\&W_0=m_0(\alpha)\left[\tau(s)-\tau_0(s)\right],\end{aligned} \tag{S19}$$

where $B(\alpha)$ is the bending stiffness and $C(\alpha)$ the torsion rigidity, which are both functions of the helical angle of the cellulose fibril helix, $\alpha$, and $\kappa_0(s)$ and $\tau_0(s)$ are the initial curvature and the initial torsion of the tendril filament, respectively.

equations S18 and S19 can be rewritten as

$$\Pi=\int_0^{L_0}\left[Q_0-Q_1\kappa(s)-Q_2\tau(s)+Q_3\kappa(s)^2+Q_4\tau(s)^2\right]\mathrm{d}s, \tag{S20}$$

where

$$Q_0 = \tfrac{1}{2}B(\alpha)\kappa_0^2 + \tfrac{1}{2}C(\alpha)\tau_0^2 + m_0(\alpha)\tau_0,\ \ Q_1 = B(\alpha)\kappa_0,$$
$$Q_2 = C(\alpha)\tau_0 + m_0(\alpha),\quad Q_3 = \tfrac{1}{2}B(\alpha),\ \ Q_4 = \tfrac{1}{2}C(\alpha). \tag{S21}$$

## S4 Shape equations of the tendril helix

For the deformation and shape formation of a tendril filament, the equilibrium and stability of a tendril with spatial configuration require that

$$\Pi \le 0,\ \delta\Pi = 0,\ \ \delta^2\Pi \ge 0, \tag{S22}$$

where $\delta x$ denotes the variation of $x$, and

$$\delta\Pi = \int \frac{\partial H_0}{\partial \kappa}\delta\kappa \mathrm{ds} + \int \frac{\partial H_0}{\partial \tau}\delta\tau \mathrm{ds} + \int H_0 \delta \mathrm{ds}. \tag{S23}$$

Based on equation S23 and using the calculus of variation[5-7], we obtain the following shape equations for a deformed tendril filament:

$$\begin{aligned} &-Q_0\kappa + Q_1\tau^2 - Q_2\kappa\tau + Q_3\kappa^3 + (3Q_4 - 2Q_3)\kappa\tau^2 + 2Q_3\kappa_{ss} \\ &+4Q_4(\frac{\tau_s}{\kappa})\tau + Q_4\frac{2\tau_s^2}{\kappa} = 0, \end{aligned} \tag{S24}$$

$$\begin{aligned} &-Q_1\tau_s + Q_2\kappa_s + 2(2Q_3 - Q_4)\kappa_s\tau + 2(Q_3 - Q_4)\kappa\tau_s \\ &+2Q_4\frac{\tau^2\tau_s}{\kappa} - 2Q_4(\frac{\tau_s}{\kappa})_{ss} = 0 \end{aligned} \tag{S25}$$

where $\kappa_s = \dfrac{\mathrm{d}\kappa}{\mathrm{ds}}$, $\tau_s = \dfrac{\mathrm{d}\tau}{\mathrm{ds}}$, $\kappa_{ss} = \dfrac{\mathrm{d}^2\kappa}{\mathrm{ds}^2}$, and $\tau_{ss} = \dfrac{\mathrm{d}^2\tau}{\mathrm{ds}^2}$.

For a tendril helix with a constant curvature and a constant twist, equation S25 is automatically satisfied. Thus equation S24 is rewritten as

$$\begin{aligned} &Q_0R^2 - Q_1R\sin^2\varphi + Q_2R\sin\varphi\cos\varphi - Q_3\cos^4\varphi \\ &+(2Q_3 - 3Q_4)\sin^2\varphi\cos^2\varphi = 0 \end{aligned} \tag{S26}$$

where $R$ and $\varphi$ are the helical radius and the helical angle, respectively.

For a helix, we have

$$\kappa = \frac{\cos^2\varphi}{R}, \quad \tau = \frac{\sin\varphi\cos\varphi}{R}. \tag{S27}$$

In addition, the curvature and the twist can also be expressed by the helical radius and the helical pitch as

$$\kappa = \frac{R}{R^2 + h_0^2}, \quad \tau = \frac{h_0}{R^2 + h_0^2}. \tag{S28}$$

Then the shape equation in equation S26 can be rewritten as

$$\begin{aligned} &Q_0 R(R^2 + h_0^2)^2 - Q_1 h_0^2(R^2 + h_0^2) + Q_2 R h_0(R^2 + h_0^2) - Q_3 R^3 \\ &+(2Q_3 - 3Q_4) R h_0^2 = 0 \end{aligned} \tag{S29}$$

**References**


1. Whitman, A. B. & DeSilva, C. N. An exact solution in a nonlinear theory of rods. *J. Elasticity* 4: 265−280 (1974).
2. Wang, J. S., Wang, G. F., Feng, X. Q. & Qin, Q. H. Surface effects on the superelasticity of nanohelices. *J. Phys. Condens. Matter* 24: 265303 (2012).
3. Marklund, E. & Varna, J. Modeling the effect of helical fiber structure on wood fiber composite elastic properties. *Appl. Compos. Mater.* 16: 245−262 (2009).
4. Liu, Y. Z. *Nonlinear mechanics of thin elastic rod: theoretical basics of mechanical model of DNA* (Tsinghua University Press, Beijing, 2006).
5. Wang, J. S., Ye, H. M., Qin, Q. H., Xu, J. & Feng, X. Q. Anisotropic surface effects on the formation of chiral morphologies of nanomaterials. *Proc. R. Soc. A* 468: 609−633 (2012).
6. Tu, Z. C., Li, Q. X. & Hu, X. Theoretical determination of the necessary conditions for the formation of ZnO nanorings and nanohelices. *Phy. Rev. B* 73: 115402 (2006).
7. Gao, L.T., Feng, X.Q., Yin, Y. J. & Gao, H. J. An electromechanical liquid crystal

model of vesicles. *J. Mech. Phys. Solids* 59: 2844-2862 (2008).